Dynamical transition between synchronization and antisynchronization with exceptional points

Kun-Jie Zhou, Jian Zou [*] and Bin Shao

School of Physics, Beijing Institute of Technology, Beijing 100081, China

In this paper we consider a spin chain locally coupled to dissipative environments with unbalanced gain and loss and explore the relation between the emergence of synchronization and exceptional points. For our model in the Liouvillian formalism the matrix of the Liouvillian superoperator is block diagonal and the different blocks correspond to the dynamics of different observables. We find that for $\hat{\sigma}^z$ corresponding to the block having a single Liouvillian exceptional point (LEP), when the coupling strength between the nearest spins is beyond the LEP, the synchronization or antisynchronization will occur. For $\hat{\sigma}^x$ and $\hat{\sigma}^y$ corresponding to the block having two LEPs, when the coupling strength between the nearest spins is beyond both LEPs, the synchronization or antisynchronization will appear, and as time evolves the dynamical transition between synchronization and antisynchronization can occur. Moreover, we also find that the initial state of the system does not affect the emergence of synchronization or antisynchronization, but it determines whether the system is synchronized or antisynchronized and affects the time at which the dynamical transition between synchronization and antisynchronization occurs. Furthermore, by postselecting the quantum trajectories without quantum jump, the system can exhibit Hamiltonian exceptional points, and we find that quantum jumps play an important role in the synchronization of the system.

I. INTRODUCTION

Synchronization is a fundamental phenomenon that describes the coupled objects spontaneously phase locking to a common frequency [1]. Since the first observation by Huygens in the 17th century [2], the phenomenon of synchronization has been widely observed in different systems [3–5]. The phenomenon of synchronization has been thoroughly investigated in classical systems and developed into the quantum regime recently [6,7]. In the past few years, quantum synchronization has attracted much attention and has been investigated in different systems, including two-level systems [8–15], van der Pol oscillators [16–19], ensembles of atoms [20,21], optomechanical system [22], cold ions in microtraps [23], etc. Recently, synchronization in the quantum regime has been observed experimentally [24,25]. Meanwhile, quantum synchronization has been applied to different areas, such as quantum computation [25], quantum communication [26], and quantum heat engine [27].

In open quantum systems, dissipation characterizes the progressive loss of energy, coherence, and information into the environment, and it is an important factor attributed to the emergence of synchronization [28,29]. Generally, under the weak coupling assumption between system and environment, the dynamics of the open quantum system can be described by a Lindblad master equation captured by a Liouvillian superoperator [30]. The eigenvalues of the Liouvillian superoperator characterize the modes governing the dissipative dynamics. The synchronization of the system is induced by

the timescale separation among the decay rates described by the real parts of the eigenvalues of the Liouvillian superoperator. Specifically, when the decay mode with the slowest decay rate survives while the others quickly approach zero, the phenomenon of synchronization emerges [12,13]. Different forms of dissipation and decoherence have been considered in the investigation of synchronization, including Markovian [14,15] and non-Markovian dissipative environments [31,32].

The evolution of the open quantum system is a non-Hermitian process due to the dissipation to the environment [33–35]. The presence of exceptional points (EPs) is a typical feature of non-Hermitian physics which has attracted much attention in the last two decades [36]. Such points are defined as the special points in the parameter space of a non-Hermitian system at which the eigenvalues and the corresponding eigenvectors of the non-Hermitian Hamiltonian (NHH) simultaneously coalesce [37], called Hamiltonian EPs (HEPs). The presence of EPs leads to a lot of nontrivial phenomena such as enhanced response to perturbations [38–42], asymmetric backscattering [43,44], and loss-induced lasing [45].

The Lindblad master equation which describes the evolution of the open system consists of a Hermitian free evolution part and a non-Hermitian dissipative evolution part [46]. According to quantum trajectory theory, supposing the effect of the environment on the system is continuously and perfectly probed, the Lindblad master equation is regarded as average over infinite quantum trajectories [47]. Thus, the dissipation of the system can be divided into two parts, specifically, the nonunitary evolution of the system and the quantum jumps caused by the continuous measurement performed by the environment on the system [48–50]. Quantum jumps induce

---
[*]zoujian@bit.edu.cn

a random and instantaneous change of the stochastic wave function describing the system [49]. In the quantum regime, the effect of quantum jumps can be ignored by postselecting the quantum trajectories where no quantum jump occurs [47,51,52]. The majority of studies focus on the HEPs of the effective non-Hermitian Hamiltonian describing the evolution of the open system without quantum jumps [53,54]. However, the inclusion of quantum jumps can have a profound effect on the system dynamics [50]. Recently, the EPs of the systems taking into account the effect of quantum jumps have been considered in different systems [55–57], which are defined via the degeneracies of the non-Hermitian Liouvillian superoperator, called Liouvillian EPs (LEPs). The system exhibits LEPs when two or more eigenvalues and the corresponding eigenmatrices of the Liouvillian superoperator coalesce simultaneously. The point in the parameter space where n eigenvalues and the corresponding eigenmatrices coalesce corresponds to the nth-order LEP [50].

Due to the emergence of synchronization and the emergence of LEPs, which are both relative to the eigenspectrum of Liouvillian superoperators, it is intuitively expected that there might be some connection between them. However, to the best of our knowledge, little is known about the relation between the emergence of synchronization and the LEPs. There was so far only one study in this direction; specifically, Cabot *et al.* showed two distinct scenarios in which synchronization can emerge, related respectively to the presence of a nondegenerate long-lived eigenmode and to the presence of a single-frequency regime in their recent work [13].

In this paper, we investigate the synchronization of a spin chain coupled to dissipative environments locally with unbalanced gain and loss. We demonstrate the eigenspectrum of the Liouvillian superoperator governing the dynamics of the system and find that the system exhibits LEPs. Due to the block structure of the Liouvillian superoperator, the dynamics of different observables are related to different blocks of the Liouvillian superoperator. For $\hat{\sigma}^z$ corresponding to the block with a single LEP, when the coupling strength between the nearest spins is greater than the LEP it could get synchronized or antisynchronized. For $\hat{\sigma}^x$ and $\hat{\sigma}^y$ corresponding to the blocks with two LEPs, when the coupling strength between the nearest spins is greater than both LEPs it could get synchronized or antisynchronized, and as time evolves the dynamical transition between synchronization and antisynchronization could occur. Moreover, we find that the initial state of the system does not affect the emergence of (anti)synchronization between the spins, but it would determine whether the system is synchronized or antisynchronized and when the dynamical transition between synchronization and antisynchronization occurs. Furthermore, by postselecting the quantum trajectories where no quantum jump occurs, we find that the system can exhibit HEPs. When the coupling strength is greater than the HEP, the system remains synchronized or antisynchronized in the whole evolution. Comparing the synchronization with these two kinds of EPs, we find that quantum jumps play an important role in the synchronization of the system.

The rest of this paper is organized as follows. In Sec. II we introduce the model considered in this paper. In Sec. III A we discuss the connection between the emergence of

synchronization and LEPs, and explore the effect of the initial state of the system on synchronization. In Sec. III B we study the synchronization in the absence of quantum jumps, and discuss the connection between the emergence of synchronization and HEPs. And Sec. IV is the conclusion.

II. MODEL

In this paper, we consider a one-dimensional Heisenberg *XX* spin chain consisting of two spins, and each spin is coupled to a local dissipative bath. The Hamiltonian of our model is

$$\hat{H} = \kappa\big(\hat{\sigma}_1^x \hat{\sigma}_2^x + \hat{\sigma}_1^y \hat{\sigma}_2^y\big), \tag{1}$$

where κ is the coupling strength between the spins, and $\hat{\sigma}_j^x$, $\hat{\sigma}_j^y$ $(j = 1, 2)$ are the Pauli operators. For convenience we set $\hbar = 1$. With the Markovian approximation, when the open quantum system is weakly interacting with the baths, the time evolution of the system density matrix is described by the following Lindblad master equation [30,58]:

$$\dot{\rho} = -i[\hat{H}, \rho] + \sum_{m=1}^{4}(2\hat{L}_m \rho \hat{L}_m^\dagger - \hat{L}_m^\dagger \hat{L}_m \rho - \rho \hat{L}_m^\dagger \hat{L}_m), \tag{2}$$

where

$$\hat{L}_{1,2} = \tfrac{1}{2}\sqrt{\gamma_1(1 \pm \mu)}\hat{\sigma}_1^\pm, \quad \hat{L}_{3,4} = \tfrac{1}{2}\sqrt{\gamma_2(1 \mp \mu)}\hat{\sigma}_2^\pm \tag{3}$$

are four symmetric Lindblad operators acting on the spins, and $\hat{\sigma}_j^\pm = (\hat{\sigma}_j^x \pm i\hat{\sigma}_j^y)/2$ $(j = 1, 2)$ are the raising and lowering operators. The parameters γ_1 and γ_2 determine the dissipative strength of different spins, and $\mu \in [-1, 1]$ is the driving parameter which characterizes the magnetization bias between the left and the right baths. This model is simple in concept and has been studied deeply in recent years, especially in the limiting case $\mu = 1$ where the left (right) bath only induces down-up (up-down) spin flips [58–60]. In the case of $\mu = 1$, the left and the right baths can be regarded as in two oppositely polarized ferromagnets. For $\mu = 1$, the dynamics of the system is simplified as

$$\dot{\rho} = -i[\hat{H}, \rho] + \gamma_1 \mathcal{D}[\hat{\sigma}_1^+]\rho + \gamma_2 \mathcal{D}[\hat{\sigma}_2^-]\rho. \tag{4}$$

The dissipative nature of the system includes the gain of the left bath and the loss of the right bath, which is described by the dissipative superoperators in the Lindblad form $\mathcal{D}[\hat{o}]\rho = \hat{o}\rho\hat{o}^\dagger - \{\hat{o}^\dagger\hat{o}, \rho\}/2$, and the corresponding gain rate and loss rate are γ_1 and γ_2, respectively. The model of a spin chain interacting with two baths independently at two ends is widely used in the investigation of spin chains with open boundary condition [61–65].

It is convenient to describe the dynamical evolution in the Liouvillian representation. The above master equation can be expressed as $\dot{\rho} = \mathcal{L}\rho$, where $\mathcal{L}$ is the Liouvillian superoperator. In the Liouvillian representation, the density matrix is represented by a vector in the Hilbert-Schmidt space and $\mathcal{L}$ is a non-Hermitian matrix. And a D-dimensional density matrix is represented by a D^2-dimensional vector

$$|\rho\rangle\rangle = (\rho_1 \ \rho_2 \ \dots \ \rho_{D^2})^T, \tag{5}$$

where T denotes the transpose operation. Then we can recast the above master equation Eq. (4) as a matrix differential

equation for vectorized state $|\rho\rangle\rangle$ of the density operator ρ:

$$\dot{\rho} = \mathcal{L}\rho \longleftrightarrow |\dot{\rho}\rangle\rangle = \mathcal{L}|\rho\rangle\rangle. \qquad (6)$$

Then $\mathcal{L}$ can be written as a $(D^2 \times D^2)$-dimensional matrix. Explicitly, the matrix form of $\mathcal{L}$ of Eq. (6) is given by

$$
\begin{aligned}
\mathcal{L} = & -i(H \otimes \mathbb{1} - \mathbb{1} \otimes H^T) \\
& + \gamma_1\{\hat{\sigma}_1^+ \otimes (\hat{\sigma}_1^-)^T - \tfrac{1}{2}[\hat{\sigma}_1^- \hat{\sigma}_1^+ \otimes \mathbb{1} + \mathbb{1} \otimes (\hat{\sigma}_1^- \hat{\sigma}_1^+)^T]\} \\
& + \gamma_2\{\hat{\sigma}_2^- \otimes (\hat{\sigma}_2^+)^T - \tfrac{1}{2}[\hat{\sigma}_2^+ \hat{\sigma}_2^- \otimes \mathbb{1} + \mathbb{1} \otimes (\hat{\sigma}_2^+ \hat{\sigma}_2^-)^T]\}.
\end{aligned}
$$

$$(7)$$

Since the Liouvillian superoperator is non-Hermitian, its eigenvalue spectrum has distinct right and left eigenmatrices, which are defined by $\mathcal{L}\rho_i = \lambda_i \rho_i$ and $\mathcal{L}^\dagger \sigma_i = \lambda_i^* \sigma_i$, respectively. The right and left eigenmatrices form a biorthogonal basis with respect to the Hilbert-Schmidt inner product, which can be normalized by $\mathrm{Tr}[\sigma_i \rho_j] = \delta_{ij}$. From such definition, the steady state of the system ρ_{SS} corresponds to the eigenmatrix with eigenvalue $\lambda_i = 0$. If two or more eigenvalues and eigenmatrices coalesce simultaneously, LEPs emerge. As a result of the symmetry on the superoperator level, Eq. (7) can be decomposed into five different blocks, $\mathcal{L} = \oplus_\nu \mathcal{L}_\nu$, with $\nu \in \{a, b, c, d, e\}$ [66]. The explicit forms of the divided Liouvillian superoperators are provided in Appendix A. In this way, the complexity of the calculation of the Liouvillian spectrum can be greatly reduced.

In the Liouvillian formalism, if a Liouvillian superoperator is diagonalizable, the general solution of the master equation can be expressed as a weighted sum of the right eigenmatrices ρ_i with exponentially decaying factors:

$$\rho(t) = \sum_{i=1} c_i e^{\lambda_i t} \rho_i, \qquad (8)$$

where $c_i = \mathrm{Tr}[\sigma_i \rho(0)]$, which is connected to the initial state of the system. Therefore, the real part and the imaginary part of the eigenvalues λ_i are responsible for the decay rates and the oscillations of any expectation value towards the steady state, respectively.

III. RESULT

A. Liouvillian exceptional points

It is known that the emergence of synchronization is rooted in the timescale separation among the decay rates of the oscillations in the local observables, which are described by the real parts of the eigenvalues of the Liouvillian superoperator governing the dynamics [28]. In the general scenario of synchronization, two detuned qubits interact with each other under collective dissipation, and the emergence of synchronization can be observed when the decay mode with the slowest decay rate survives while the others quickly approach zero [15]. Additionally, synchronization can also be achieved in the scenario of both identical qubits under local dissipation at different dissipative strength [12,21]. In this paper, we consider a two-spin chain locally coupled to dissipative baths with unbalanced gain and loss. The imbalance of the local dissipation would break the symmetry of the system and lead to nontrivial synchronization.

In general, for the system composed of spins, the expectation values of Pauli operators are used as the local observables to monitor the dynamics of synchronization. First, we choose the expectation value of $\hat{\sigma}^x$ as the local observable to characterize the synchronization between the spins. In the Liouvillian representation, from Eq. (8), the local observable $\langle \hat{\sigma}_j^x(t) \rangle$ can be expressed as

$$\langle \hat{\sigma}_j^x(t) \rangle = \mathrm{Tr}[\hat{\sigma}_j^x \rho] = \sum_{i=1}^{16} c_i \mathrm{Tr}[\hat{\sigma}_j^x \rho_i] e^{\lambda_i t}, \qquad (9)$$

where $j = 1, 2$ denotes two different system spins. From calculation, it can be found that only $\mathrm{Tr}[\hat{\sigma}_j^x \rho_i^b]$ and $\mathrm{Tr}[\hat{\sigma}_j^x \rho_i^c]$ are nonzero. Meanwhile, due to $\mathcal{L}_b = \mathcal{L}_c^*$, the expression of $\langle \hat{\sigma}_j^x(t) \rangle$ can be simplified and only the spectrum of $\mathcal{L}_b$ is concerned:

$$\langle \hat{\sigma}_j^x(t) \rangle = 2 \sum_{i=1}^{4} c_i^b \mathrm{Tr}[\hat{\sigma}_j^x \rho_i^b] e^{\lambda_i^b t}, \qquad (10)$$

where $c_i^b = \mathrm{Tr}[\sigma_i^b \rho(0)]$, and λ_i^b and ρ_i^b are the eigenvalues and right eigenmatrices of $\mathcal{L}_b$, respectively. The concrete expression of λ_i^b is shown as follows:

$$\lambda_{1,2}^b = -\Gamma \pm \frac{\sqrt{2}}{4}\sqrt{\alpha - \beta}, \quad \lambda_{3,4}^b = -\Gamma \pm \frac{\sqrt{2}}{4}\sqrt{\alpha + \beta}, \qquad (11)$$

where

$$
\begin{aligned}
\Gamma &= (\gamma_1 + \gamma_2)/2, \\
\alpha &= \gamma_1^2 + \gamma_2^2 - 32\kappa^2, \\
\beta &= \sqrt{(\gamma_1^2 - \gamma_2^2)^2 - 64(\gamma_1^2 - 6\gamma_1\gamma_2 + \gamma_2^2)\kappa^2}. \qquad (12)
\end{aligned}
$$

And the explicit expression of the right eigenmatrices ρ_i^b corresponding to the above eigenvalues λ_i^b is given in Appendix B.

It can be seen from the Liouvillian spectrum of $\mathcal{L}_b$ that different eigenvalues and eigenmatrices are coalesced under certain conditions, which manifests the existence of LEPs. According to Eq. (11), when $\alpha - \beta = 0$, $\lambda_1^b = \lambda_2^b$, and as shown in Appendix B the corresponding eigenmatrices $\rho_1^b = \rho_2^b$, which indicates a second-order LEP. When $\alpha + \beta = 0$, $\lambda_3^b = \lambda_4^b$, and the corresponding eigenmatrices $\rho_3^b = \rho_4^b$ (see Appendix B), which indicates another second-order LEP.

For fixed dissipative strength γ_1 and γ_2, when the value of coupling strength between the spins κ satisfies one of the following conditions,

$$\kappa_1^b = \tfrac{1}{4}(\sqrt{2} - 1)\sqrt{\gamma_1\gamma_2} \quad (\alpha - \beta = 0), \qquad (13)$$

$$\kappa_2^b = \tfrac{1}{4}(\sqrt{2} + 1)\sqrt{\gamma_1\gamma_2} \quad (\alpha + \beta = 0), \qquad (14)$$

the LEP appears. Both types of LEPs can be reached for a large range of parameters. Meanwhile, it should be noted that the two types of LEPs cannot be reached simultaneously for fixed γ_1 and γ_2.

In Fig. 1, we show the Liouvillian spectrum for different values of coupling strength corresponding to the LEPs. For $\gamma_1 = 0.02$ and $\gamma_2 = 0.01$, it can be directly obtained that $\kappa_1^b \approx 0.001\,464$ and $\kappa_2^b \approx 0.008\,536$, corresponding to
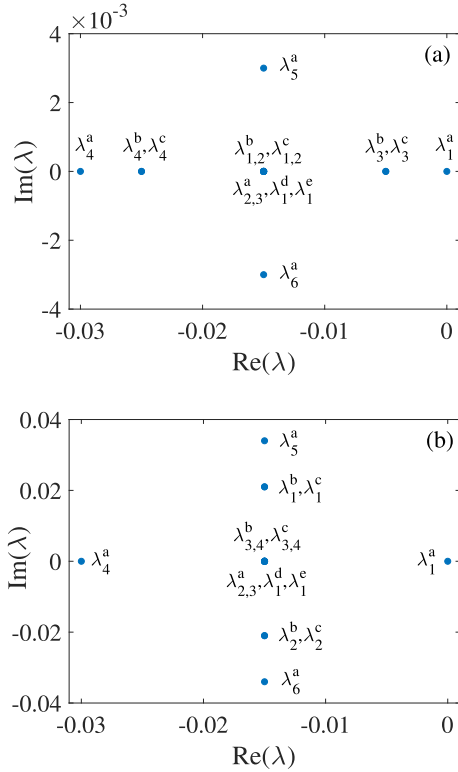
FIG. 1. The Liouvillian eigenvalue spectrum $\{\lambda_i\}$ with different κ at LEPs. The horizontal axis denotes the real part of λ_i, and the vertical axis denotes the imaginary part of λ_i. (a) $\kappa \approx 0.001\,464$. (b) $\kappa \approx 0.008\,536$. We set $\gamma_1 = 0.02$, $\gamma_2 = 0.01$.

$\alpha - \beta = 0$ and $\alpha + \beta = 0$, respectively. It can be seen from Fig. 1(a) that, for $\kappa = \kappa_1^b \approx 0.001\,464$, eigenvalues $\lambda_{1,2}^b = \lambda_{1,2}^c = \lambda_{2,3}^a = \lambda_1^d = \lambda_1^e$. However, it can be seen from Appendix B that only the eigenmatrices $\rho_1^b = \rho_2^b$ and $\rho_1^c = \rho_2^c$. It indicates that there are simultaneously two second-order LEPs for $\kappa = \kappa_1^b$. Furthermore, in Fig. 1(a), $\lambda_3^b = \lambda_3^c$ and $\lambda_4^b = \lambda_4^c$, but the corresponding eigenmatrices are not coalesced. As is shown in Fig. 1(b), for $\kappa = \kappa_2^b = 0.008\,536$, $\sqrt{\alpha - \beta}$ becomes imaginary, and eigenvalues $\lambda_1^b = \lambda_1^c$ and $\lambda_2^b = \lambda_2^c$, which have two opposite nonzero imaginary parts, but the corresponding eigenmatrices $\rho_1^b \neq \rho_1^c$ and $\rho_2^b \neq \rho_2^c$. Meanwhile, eigenvalues $\lambda_{3,4}^b = \lambda_{3,4}^c = \lambda_{2,3}^a = \lambda_1^d = \lambda_1^e$. The corresponding eigenmatrices $\rho_3^b = \rho_4^b$ and $\rho_3^c = \rho_4^c$, and there are simultaneously two second-order LEPs.

It has been mentioned that $\langle \hat{\sigma}_j^x(t) \rangle$ is only determined by the eigenvalues of $\mathcal{L}_b$ [see Eq. (10)]. Specifically, the decay rates of $\langle \hat{\sigma}_j^x(t) \rangle$ are characterized by the real parts of λ_i^b, and the oscillation frequencies are characterized by the imaginary parts of λ_i^b. From Eqs. (10) and (11), it can be inferred that, when $\alpha - \beta < 0$, the eigenvalues λ_i^b are all real, and the dynamics of $\langle \hat{\sigma}_j^x(t) \rangle$ has no oscillation. When $\alpha - \beta < 0 < \alpha + \beta$, $\lambda_{1,2}^b$ are complex and the imaginary parts $\text{Im}(\lambda_1^b) = -\text{Im}(\lambda_2^b)$, thus the dynamics of $\langle \hat{\sigma}_j^x(t) \rangle$ has a unique oscillation frequency. And when $\alpha + \beta > 0$, the eigenvalues λ_i^b are all complex and the imaginary parts $\text{Im}(\lambda_1^b) = -\text{Im}(\lambda_2^b)$ and $\text{Im}(\lambda_3^b) = -\text{Im}(\lambda_4^b)$, thus the dynamics of $\langle \hat{\sigma}_j^x(t) \rangle$ has two different oscillation frequencies. It indicates that the

oscillation of the dynamics of $\langle \hat{\sigma}_j^x(t) \rangle$ is determined by $\alpha - \beta$ and $\alpha + \beta$.

In Fig. 2, we show the dynamics of $\langle \hat{\sigma}_j^x(t) \rangle$ with different interaction strength κ. We suppose that the initial state of the system is $\frac{1}{\sqrt{2}}(|g\rangle + |e\rangle) \otimes \frac{1}{\sqrt{2}}(|g\rangle + |e\rangle)$. It can be seen from Fig. 2(a) that $\langle \hat{\sigma}_1^x \rangle$ and $\langle \hat{\sigma}_2^x \rangle$ decrease as time evolves, and there is no oscillation during the decay. It has been shown that, for $\kappa = 0.001 < \kappa_1^b$, λ_i^b is real and the dynamics of $\langle \hat{\sigma}_j^x(t) \rangle$ has no oscillation. It can be seen from Fig. 2(b) that $\langle \hat{\sigma}_1^x(t) \rangle$ and $\langle \hat{\sigma}_2^x(t) \rangle$ decrease to zero with a unapparent damped oscillation during the time evolution. This is because, for $\kappa_1^b < \kappa = 0.005 < \kappa_2^b$, $\lambda_{1,2}^b$ is complex and $\lambda_{3,4}^b$ is real. However, the imaginary part of $\lambda_{1,2}^b$ is small compared with the real part of $\lambda_{1,2}^b$ and decay plays a major role in the evolution of $\langle \hat{\sigma}_j^x \rangle$. With the further increasing of κ, the imaginary part of $\lambda_{1,2}^b$ increases gradually and eventually is greater than the real part of $\lambda_{1,2}^b$. Meanwhile, the imaginary part of $\lambda_{3,4}^b$ becomes nonzero when $\kappa > \kappa_2^b$. In the rest of this paper, we label $\omega_1 = \text{Im}(\lambda_1^b)$, $\omega_2 = \text{Im}(\lambda_3^b)$. As shown in Appendix C, in this case, $\langle \hat{\sigma}_j^x \rangle$ would display two different oscillation frequencies, and in general synchronization is not able to occur. It can be seen from Fig. 2(c) that $\langle \hat{\sigma}_1^x \rangle$ and $\langle \hat{\sigma}_2^x \rangle$ do not synchronize in the decaying evolution. However, with the further increasing of κ, synchronization is able to occur. In Fig. 2(d), we plot the time evolution of $\langle \hat{\sigma}_1^x \rangle$ and $\langle \hat{\sigma}_2^x \rangle$ with a larger coupling strength $\kappa = 0.1$, and the insets show the detailed display of the oscillation of $\langle \hat{\sigma}_1^x \rangle$ and $\langle \hat{\sigma}_2^x \rangle$ for two different time intervals. It can be seen from Fig. 2(d) that $\langle \hat{\sigma}_1^x \rangle$ and $\langle \hat{\sigma}_2^x \rangle$ decay to zero after a damped oscillation. And surprisingly, as time evolves the two spins change from synchronized to antisynchronized and after a while change from antisynchronized back to synchronized again, i.e., a dynamical transition between synchronization and antisynchronization occurs.

Why do the spins get (anti)synchronized even if the local observable $\langle \hat{\sigma}_j^x \rangle$ displays two different oscillation frequencies? And what makes the dynamical transition between synchronization and antisynchronization occur? In order to clarify these questions, we tend to characterize the signatures of synchronization between the local observables of the systems quantitatively, and further analyze the synchronization phenomenon. The Pearson coefficient C_{12} is a useful tool to measure the degree of linear correlation between two time-dependent variables, which is usually used as a figure of merit to characterize the signatures of synchronization [11]. Given variables x and y, the Pearson coefficient is defined as

$$C_{12} = \frac{\overline{\delta x \delta y}}{\sqrt{\overline{\delta x^2}\,\overline{\delta y^2}}},\tag{15}$$

where $\delta x = x - \bar{x}$, and the bar stands for the time average over the time interval Δt:

$$\bar{x} = \frac{1}{\Delta t}\int_t^{t+\Delta t} x(t')dt'.\tag{16}$$

The Pearson coefficient $C_{12} = 0$ indicates that there is no synchronization, $C_{12} = 1$ indicates synchronization, and $C_{12} = -1$ indicates antisynchronization.

In Fig. 3, we plot the time evolution of the Pearson coefficient between the local observables $\langle \hat{\sigma}_1^x \rangle$ and $\langle \hat{\sigma}_2^x \rangle$. The system
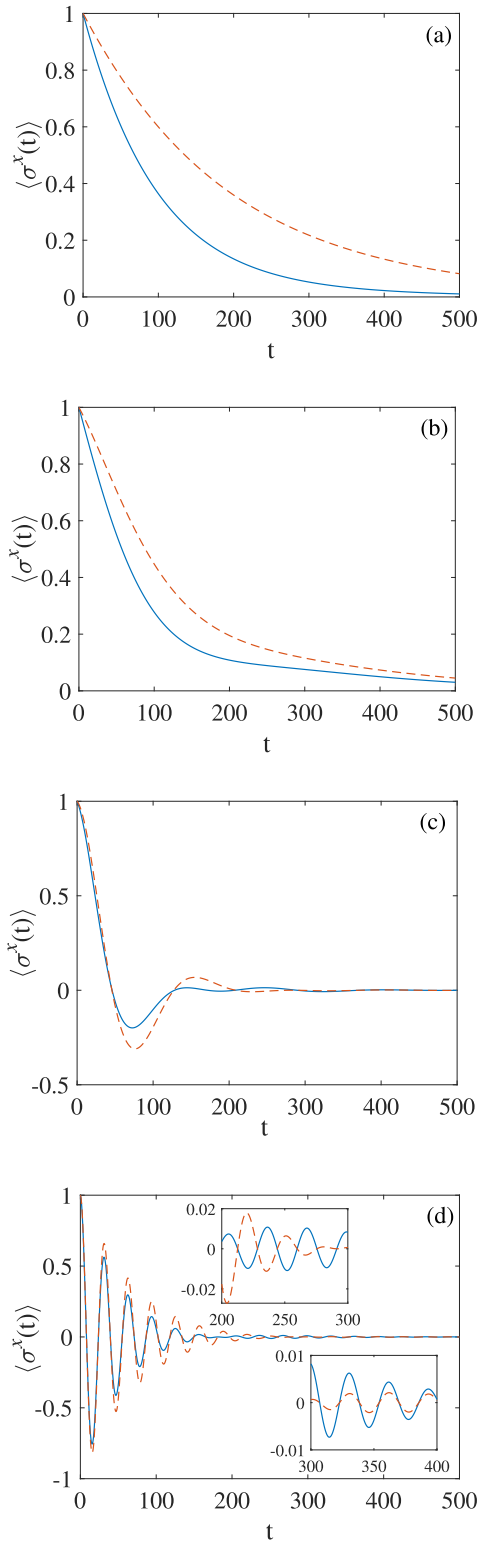
FIG. 3. Time evolution of the Pearson coefficient. The system parameters are the same as those in Fig. 2(d).

FIG. 2. The diagram of the local observable $\langle \hat{\sigma}_j^x \rangle$ as a function of t for different κ. The blue solid lines and orange dashed lines characterize $\langle \hat{\sigma}_1^x(t) \rangle$ and $\langle \hat{\sigma}_2^x(t) \rangle$, respectively. (a) $\kappa = 0.001$. (b) $\kappa = 0.005$. (c) $\kappa = 0.02$. (d) $\kappa = 0.1$. We set $\gamma_1 = 0.02$, $\gamma_2 = 0.01$. The insets of (d) show the detailed displays of the oscillation of $\langle \hat{\sigma}_1^x \rangle$ and $\langle \hat{\sigma}_2^x \rangle$ for two different time intervals.

parameters are the same as those in Fig. 2(d). It can be seen from Fig. 3 that the Pearson coefficient is 1 at the beginning,
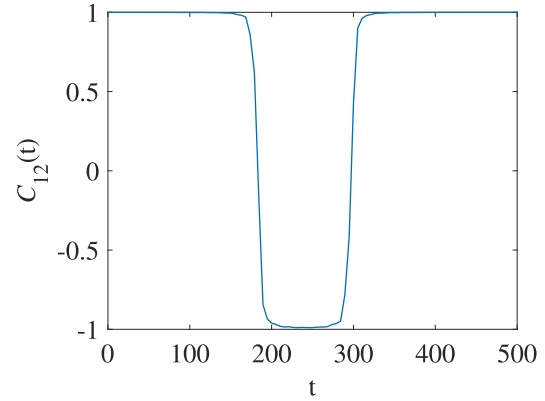
after a while it changes from 1 to -1 abruptly, and then it returns to 1 again. It means that the two spins are synchronized from the beginning and later get antisynchronized, and then the two spins get synchronized again. According to Eq. (11), we can see that with the increasing of κ, $\alpha \gg \beta$, which makes $\alpha - \beta$ and $\alpha + \beta$ approximately equal. It indicates two approximately equal imaginary parts of the eigenvalues λ_i^b and leads to two approximately equal oscillation frequencies of $\langle \hat{\sigma}_j^x \rangle$ ($\omega_1 \approx \omega_2$). In this case, $\omega_1 + \omega_2 \gg \omega_1 - \omega_2$, so we can derive from Eq. (10) that

$$\left\langle \hat{\sigma}_j^x(t) \right\rangle = \xi_j e^{-\Gamma t} \sin \left(\frac{\omega_1 + \omega_2}{2} t + \frac{\varphi_{1j} + \varphi_{2j}}{2} + \phi_j \right). \quad (17)$$

The derivation and the concrete analytical expressions of ξ_j, φ_{1j}, φ_{2j}, and ϕ_j are shown in Appendix C, where φ_{1j} and φ_{2j} are constants and ξ_j and ϕ_j are slowly varying functions of time, i.e., functions of $\frac{(\omega_1 - \omega_2)t}{2}$. It can be seen that quantum beats can be observed and the dominant oscillation frequency of the dynamics of $\langle \hat{\sigma}_j^x(t) \rangle$ is $\frac{\omega_1 + \omega_2}{2}$. This is why the spins remain (anti)synchronized during the time evolution. Though the two spins share a common oscillation frequency $\frac{\omega_1 + \omega_2}{2}$, the time-dependent coefficient ξ_j and phase ϕ_j are different for the spins. In the following, we eliminate the common decay factor $e^{-\Gamma t}$ and focus on the oscillation of $\langle \hat{\sigma}_j^x(t) \rangle$. In Fig. 4(a), we plot the time evolution of $\langle \hat{\sigma}_j^x(t) \rangle_{\text{WDF}}$, which denotes the evolution of $\langle \hat{\sigma}_j^x(t) \rangle$ without the decay factor. It can be seen from Fig. 4(a) that $\langle \hat{\sigma}_1^x(t) \rangle_{\text{WDF}}$ and $\langle \hat{\sigma}_2^x(t) \rangle_{\text{WDF}}$ change from synchronization to antisynchronization, remain antisynchronized for a while, and then change from antisynchronization to synchronization. In Figs. 4(b) and 4(c), we plot the phases ϕ_1 and ϕ_2 as functions of t. It can be seen that phase ϕ_1 abruptly changes from $\frac{\pi}{2}$ to $-\frac{\pi}{2}$ at $t \approx 180$, and ϕ_2 abruptly changes from $\frac{\pi}{2}$ to $-\frac{\pi}{2}$ at $t \approx 290$. Actually, when the coefficient ξ_j oscillates to zero, the phase ϕ_j suddenly changes from $\frac{\pi}{2}$ to $-\frac{\pi}{2}$. When the phase difference between ϕ_1 and ϕ_2 changes from zero to π, the system changes from synchronization to antisynchronization. The time interval between the sudden change of ϕ_1 and ϕ_2 makes the phase difference between ϕ_1 and ϕ_2 change from zero to π, which induces the transition between synchronization and antisynchronization.

Similar to Eq. (10), from calculation, it can be found that the dynamics of $\langle \hat{\sigma}_j^y(t) \rangle$ can also be simplified and only refers
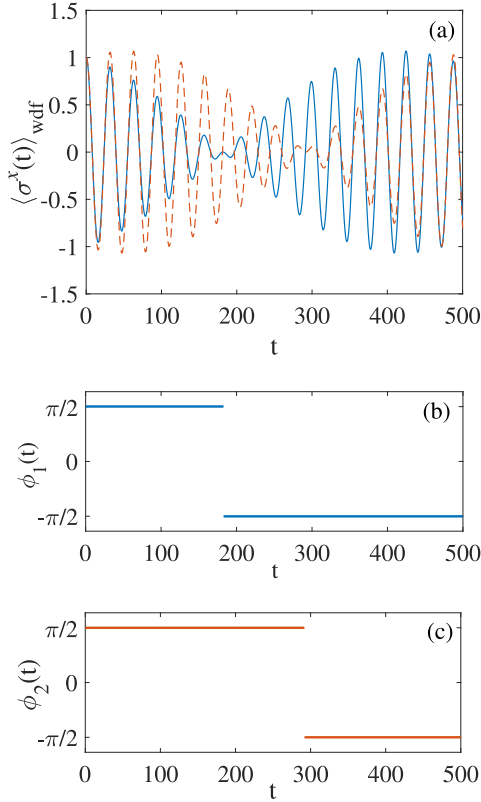
FIG. 4. (a) The time evolution of $\langle \hat{\sigma}_j^x(t) \rangle_{\text{WDF}}$. The blue solid lines and orange dashed lines characterize $\langle \hat{\sigma}_1^x(t) \rangle_{\text{WDF}}$ and $\langle \hat{\sigma}_2^x(t) \rangle_{\text{WDF}}$, respectively. (b) Phase ϕ_1 as a function of t. (c) Phase ϕ_2 as a function of t. The system parameters are the same as those in Fig. 2(d).

to the spectrum of $\mathcal{L}_b$, which can be expressed as

$$\left\langle \hat{\sigma}_j^y(t) \right\rangle = 2 \sum_{i=1}^{4} c_i^b \text{Tr}\big[\hat{\sigma}_j^y \rho_i^b\big] e^{\lambda_i^b t}, \tag{18}$$

where $c_i^b = \text{Tr}[\sigma_i^b \rho(0)]$. It indicates that the dynamics of the local observables $\langle \hat{\sigma}^x \rangle$ and $\langle \hat{\sigma}^y \rangle$ have no difference qualitatively. Therefore, we do not specify the synchronization between the spins characterized by $\langle \hat{\sigma}^y \rangle$.

Next, we choose $\langle \hat{\sigma}^z \rangle$ as the local observable to investigate the synchronization between the spins. From calculation, we find that the dynamics of $\langle \hat{\sigma}^z \rangle$ is fully governed by $\mathcal{L}_a$. Similar to Eq. (10), the local observable $\langle \sigma_j^z \rangle$ can be expressed as

$$\left\langle \hat{\sigma}_j^z(t) \right\rangle = \sum_{i=1}^{6} c_i^a \text{Tr}\big[\hat{\sigma}_j^z \rho_i^a\big] e^{\lambda_i^a t}, \tag{19}$$

where $c_i^a = \text{Tr}[\sigma_i^a \rho(0)]$, and λ_i^a and ρ_i^b are the eigenvalues and eigenmatrices of $\mathcal{L}_a$, respectively. According to the matrix expression of $\mathcal{L}_a$, the eigenvalue spectrum can be obtained as

$$\lambda_1^a = 0, \quad \lambda_{2,3}^a = -\Gamma, \quad \lambda_4^a = -2\Gamma, \quad \lambda_{5,6}^a = -\Gamma \pm \tfrac{1}{2}\eta, \tag{20}$$

where

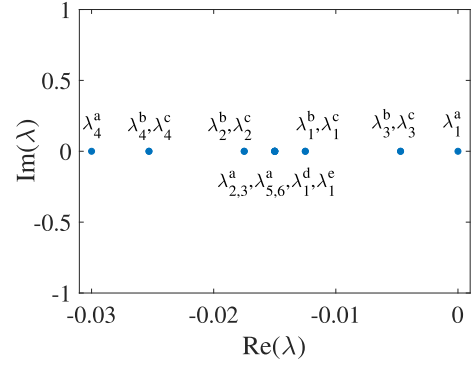$$\eta = \sqrt{(\gamma_1 - \gamma_2)^2 - 64\kappa^2}. \tag{21}$$

FIG. 5. The Liouvillian spectrum $\{\lambda_i\}$ at LEP $\kappa = 0.001\,25$. The horizontal axis denotes the real part of λ_i, and the vertical axis denotes the imaginary part of λ_i. We set $\gamma_1 = 0.02$, $\gamma_2 = 0.01$.

The explicit expressions of the right eigenmatrices ρ_i^a corresponding to the above eigenvalues λ_i^a are shown in Appendix B. It is worth mentioning that the eigenmatrix corresponding to $\lambda_1^a = 0$ characterizes the steady state of the system.

It can be seen from the Liouvillian spectrum of $\mathcal{L}_a$ that, for $\eta = 0$, eigenvalues $\lambda_{2,3}^a$ coalesce with $\lambda_{5,6}^a$. However, only the eigenmatrices ρ_5^a coalesce with ρ_6^a, which indicates a second-order LEP. For fixed dissipative strength γ_1 and γ_2, the value of coupling strength between the spins κ satisfies the following condition under which the LEP appears:

$$\kappa^a = \frac{\gamma_1 - \gamma_2}{8} \quad (\eta = 0). \tag{22}$$

This LEP can be reached for a large range of parameters. In Fig. 5, we show the Liouvillian spectrum for $\kappa = \kappa^a$. Given $\gamma_1 = 0.02$ and $\gamma_2 = 0.01$, the corresponding $\kappa^a = 0.001\,25$ for $\eta = 0$. It can be seen from Fig. 5 that all eigenvalues of the Liouvillian superoperator $\mathcal{L}$ are real. Eigenvalues $\lambda_{2,3}^a = \lambda_5^a = \lambda_6^a = \lambda_1^d = \lambda_1^e$. However, it can be seen from Appendix B that of the corresponding eigenmatrices only ρ_5^a coalesces with ρ_6^a, and there is only one second-order LEP.

As shown in Eq. (19), the dynamics of $\langle \hat{\sigma}_j^z(t) \rangle$ is determined by the eigenvalues of $\mathcal{L}_a$. Specifically, the decay rates of $\langle \hat{\sigma}_j^z(t) \rangle$ are characterized by the real parts of λ_i^a, and the oscillation frequencies are characterized by the imaginary parts of λ_i^a. From Eqs. (19) and (20) it can be seen that, when $\kappa < \kappa^a$, eigenvalues λ_i^a are real, and the dynamics of $\langle \hat{\sigma}_j^z(t) \rangle$ has no oscillation. When $\kappa > \kappa^a$, eigenvalues λ_i^a have a nonzero imaginary part, which causes the oscillation of $\langle \hat{\sigma}_j^z(t) \rangle$.

In Fig. 6, we demonstrate the dynamics of $\langle \hat{\sigma}_j^z \rangle$ for two different interaction strengths κ, and in Figs. 6(a) and 6(b) $\kappa = 0.001$ and 0.05, respectively. It can be seen from Fig. 6(a) that $\langle \hat{\sigma}_1^z \rangle$ increases as time evolves and then reaches a steady value. In contrast, $\langle \hat{\sigma}_2^z \rangle$ decreases as time evolves and then reaches a steady value. This can be explained as that, for $\kappa = 0.001 < \kappa^a$, the imaginary part of λ_i^a is zero and the dynamics of $\langle \hat{\sigma}_j^z \rangle$ has no oscillation. As shown in Fig. 6(b) $\langle \hat{\sigma}_1^z \rangle$ and $\langle \hat{\sigma}_2^z \rangle$ increase to steady values with the same frequency in antiphase oscillation, which indicates the antisynchronization between the spins. It has been shown that, for $\kappa = 0.05 > \kappa^a$, the
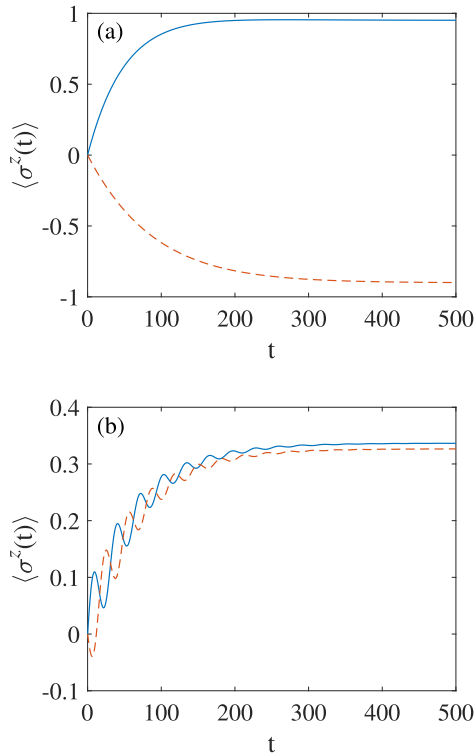
FIG. 6. The diagram of the local observable $\langle \hat{\sigma}_j^z \rangle$ as a function of t for different κ. The blue solid lines and orange dashed lines characterize $\langle \hat{\sigma}_1^z(t) \rangle$ and $\langle \hat{\sigma}_2^z(t) \rangle$, respectively. (a) $\kappa = 0.001$. (b) $\kappa = 0.05$. We set $\gamma_1 = 0.02$, $\gamma_2 = 0.01$.

imaginary parts of λ_5^a and λ_6^a are the same, and the dominant frequency of the oscillation of $\langle \hat{\sigma}_j^z \rangle$ is $\text{Im}(\lambda_{5,6}^a)$.

In the general scenario of synchronization, detuned qubits get synchronized as a result of the time separation among the decay rates of the oscillation modes in the local observables, which is induced by the presence of a common bath that filters out all the decay modes but the slowest one. However, in this paper, we consider a different scenario of synchronization of a two-spin chain under local dissipation with unbalanced gain and loss. The asymmetry of the former is induced by the detuning between the qubits, while the asymmetry of the latter is induced by the imbalance between the local dissipation. For $\langle \hat{\sigma}^z \rangle$, when the coupling strength between the spins κ is greater than the LEP, it only exhibits a single oscillation mode and thus the local observables get (anti)synchronized. And for $\langle \hat{\sigma}^x \rangle$ or $\langle \hat{\sigma}^y \rangle$, when κ is greater than the first LEP, even though the local observables exhibit a single oscillation mode, the decay plays a dominant role in the evolution and the oscillation cannot be observed. When κ is slightly greater than the second LEP, the local observables exhibit two different oscillation modes with the same decay rate, which indicates the local observables do not (anti)synchronize in the evolution. With the further increasing of κ, the two oscillation modes gradually approach each other and become approximately equal. Quantum beats can be observed and the local observables display the same dominant oscillation frequency, which indicates the emergence of synchronization. Actually, in the general synchronization scenario, if the other modes are decayed out and only the slowest mode survives, the

synchronization at this time is just like the synchronization with a single oscillation mode considered in this paper. Moreover, if the decay rates and frequencies of the two surviving slowest modes are approximately equal, and the decay rates of the other oscillation modes are significantly greater than those of the two slowest modes, the synchronization in this case is coincident with the synchronization with two approximately equal oscillation modes considered in this paper.

We have used $\frac{1}{\sqrt{2}}(|g\rangle + |e\rangle) \otimes \frac{1}{\sqrt{2}}(|g\rangle + |e\rangle)$ as the initial state of the system to investigate the relation between the emergence of synchronization and LEPs. Now we take a more general state $(\cos\theta_1 |g\rangle + \sin\theta_1 |e\rangle) \otimes (\cos\theta_2 |g\rangle + \sin\theta_2 |e\rangle)$, $\theta_1, \theta_2 \in [0, 2\pi]$ as the initial states of the system to investigate the effect of initial state on synchronization. According to Eq. (10), it can be inferred that the oscillation frequency of $\langle \hat{\sigma}_j^x \rangle$ is determined by the imaginary parts of the eigenvalues of the Liouvillian superoperator $\mathcal{L}_b$, and the effect of the initial state is included in the coefficient c_i^b. Changing the initial state of the system does not affect the oscillation frequency of $\langle \hat{\sigma}_1^x \rangle$ and $\langle \hat{\sigma}_2^x \rangle$. It can be seen from Appendix C that coefficient ξ_j and phase ϕ_j are related to the coefficient A_{ij}, and indirectly related to the coefficient c_i^b which is determined by the initial state of the system. Therefore, changing the initial state of the system would affect the values of the amplitude and the phase of the oscillation. Meanwhile, phase ϕ_j is time dependent, and the change of phase induced by the change of initial state would affect the time at which the dynamical transition between synchronization and antisynchronization occurs. In Fig. 7, we display the synchronization between $\langle \hat{\sigma}_1^x \rangle_{\text{WDF}}$ and $\langle \hat{\sigma}_2^x \rangle_{\text{WDF}}$ and the corresponding Pearson coefficient for different initial states, where the common decay factors of the local observables are omitted, and the system parameters are the same as those in Fig. 4. In Figs. 7(a) and 7(b), the initial state of the system is $(\cos\frac{\pi}{4}|g\rangle + \sin\frac{\pi}{4}|e\rangle) \otimes (\cos\frac{\pi}{3}|g\rangle + \sin\frac{\pi}{3}|e\rangle)$. It can be seen that the time at which the transition between synchronization and antisynchronization occurs has a shift compared with Fig. 4. Meanwhile, the time interval in which $\langle \hat{\sigma}_1^x \rangle_{\text{WDF}}$ and $\langle \hat{\sigma}_2^x \rangle_{\text{WDF}}$ remain antisynchronized is longer than that in Fig. 4. In Figs. 7(c) and 7(d), the initial state of the system is $(\cos\frac{\pi}{4}|g\rangle + \sin\frac{\pi}{4}|e\rangle) \otimes (\cos\frac{3\pi}{4}|g\rangle + \sin\frac{3\pi}{4}|e\rangle)$. It can be seen that $\langle \hat{\sigma}_1^x \rangle_{\text{WDF}}$ and $\langle \hat{\sigma}_2^x \rangle_{\text{WDF}}$ change from antisynchronization to synchronization and remain synchronized for a while, then change from synchronization back to antisynchronization. Compared with Fig. 4, it can be found that the (anti)synchronization in Fig. 7(d) is opposite to that in Fig. 4. In Figs. 7(e) and 7(f), the initial state of the system is $(\cos\frac{\pi}{4}|g\rangle + \sin\frac{\pi}{4}|e\rangle) \otimes (\cos\frac{\pi}{6}|g\rangle + \sin\frac{\pi}{6}|e\rangle)$. It can be seen that $\langle \hat{\sigma}_1^x \rangle_{\text{WDF}}$ and $\langle \hat{\sigma}_2^x \rangle_{\text{WDF}}$ remain synchronized in the whole evolution. It is because the change of initial state makes the phases ϕ_1 and ϕ_2 produce an identical phase change π at the same time and the phase difference between ϕ_1 and ϕ_2 remains zero. It is worth mentioning that the effect of the initial state of the system on the synchronization between $\langle \hat{\sigma}_1^y \rangle$ and $\langle \hat{\sigma}_2^y \rangle$ has no qualitative difference from that of $\langle \hat{\sigma}_1^x \rangle$.

Similarly, it can be inferred from Eq. (19) that the oscillation frequency of $\langle \hat{\sigma}^z \rangle$ is determined by the imaginary parts of the eigenvalues of the Liouvillian superoperator $\mathcal{L}_a$, and the effect of the initial state is included in the coefficient c_i^a. Changing the initial state of the system would affect the amplitude and the phase of $\langle \hat{\sigma}_j^z \rangle$. However, the phase of $\langle \hat{\sigma}_j^z \rangle$
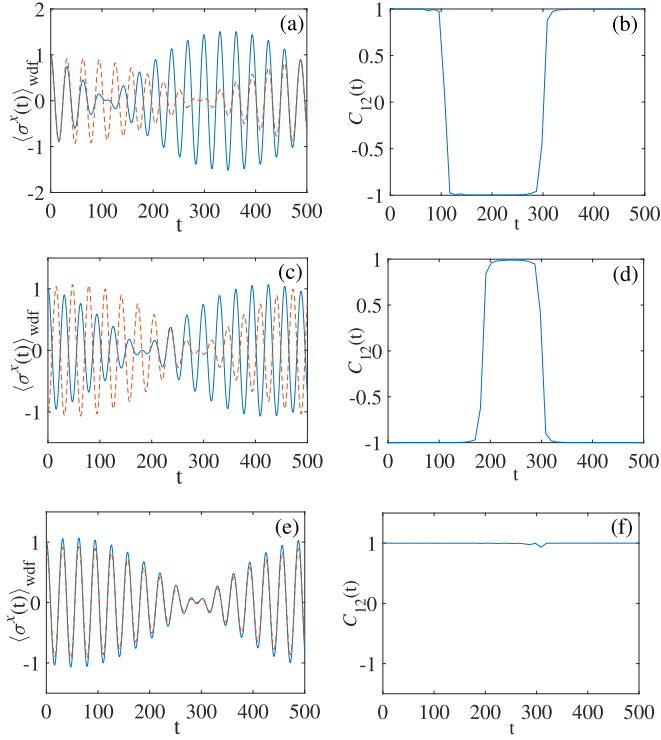
FIG. 7. (a, c, e) The time evolution of $\langle \hat{\sigma}_j^x(t) \rangle_{\text{WDF}}$ with different initial states. The blue solid lines and orange dashed lines characterize $\langle \hat{\sigma}_1^x(t) \rangle_{\text{WDF}}$ and $\langle \hat{\sigma}_2^x(t) \rangle_{\text{WDF}}$, respectively. (b, d, f) The corresponding time evolutions of the Pearson coefficient of panels (a), (c), and (e), respectively. (a, b) $\theta_1 = \frac{\pi}{4}, \theta_2 = \frac{\pi}{3}$. (c, d) $\theta_1 = \frac{\pi}{4}, \theta_2 = \frac{3\pi}{4}$. (e, f) $\theta_1 = \frac{\pi}{4}, \theta_2 = \frac{\pi}{6}$. The system parameters are the same as those in Fig. 4.

is a constant, and $\langle \hat{\sigma}_1^z \rangle$ and $\langle \hat{\sigma}_2^z \rangle$ would remain synchronized or antisynchronized in the whole evolution. The initial state of the system only determines whether the system is synchronized or antisynchronized.

As mentioned above, in the general scenario, synchronization is determined by the nature of the open-system dynamics, in which the common dissipation filters out all the oscillation modes with different decay rates but the slowest one. It can be seen from the general expression of the local observable Eq. (9) that the coefficient c_i is related to the initial state of the system, which would affect the amplitude and the phase of oscillation of the local observables quantitatively, but make no qualitative difference in synchronization. In this paper, even if we consider a different scenario, synchronization is actually determined by the property of the dynamics. Specifically, synchronization emerges when the dynamics of the local observables exhibits only a single oscillation mode or two approximately equal oscillation modes as the coupling strength between the spins is greater than the LEPs. Once the value of coupling strength between the spins is sufficient to establish (anti)synchronization, the corresponding local observables remain (anti)synchronized from the beginning of the evolution. As shown above, the emergence of (anti)synchronization is robust to the change of the initial state of the system. However, the initial state would also affect the amplitude and the phase of the oscillation, which would determine whether the system

is synchronized or antisynchronized and affect the time at which the dynamical transition between synchronization and antisynchronization occurs. It can be seen that the effect of the initial state of the system on synchronization in this paper has no qualitative difference with that in the general scenario.

B. Hamiltonian exceptional points

We have discussed the relation between the emergence of synchronization and LEPs in Sec. III A. In this subsection, we tend to study the relation between the emergence of synchronization and HEPs, and investigate the effect of quantum jumps on synchronization.

As mentioned above, the Lindblad master equation consists of a Hermitian Hamiltonian part describing the unitary evolution of the system, and non-Hermitian dissipation parts describing the progressive loss of energy, coherence, and information induced by the environment. Referring to quantum trajectory theory, supposing the effect of the environment on the system is continuously and perfectly probed, the Lindblad master equation is regarded as the average over infinite quantum trajectories [47]. Thus, the dissipation terms of the master equation can be divided into two parts: the nonunitary evolution of the system and the quantum jumps caused by the continuous measurement performed by the environment on the system [48–50]. By rearranging the terms in the Lindblad master equation, Eq. (4) can be rewritten as

$$
\begin{aligned}
\dot{\rho} &= -i[\hat{H}, \rho] + \gamma_1 \mathcal{D}[\hat{\sigma}_1^+]\rho + \gamma_2 \mathcal{D}[\hat{\sigma}_2^-]\rho \\
&= -i(\hat{H}_{\text{eff}}\rho - \rho \hat{H}_{\text{eff}}^\dagger) + \gamma_1 \hat{\sigma}_1^+ \rho \hat{\sigma}_1^- + \gamma_2 \hat{\sigma}_2^- \rho \hat{\sigma}_2^+,
\end{aligned} \quad (23)
$$

where

$$
\hat{H}_{\text{eff}} = \hat{H} - \frac{i\gamma_1}{2}\hat{\sigma}_1^- \hat{\sigma}_1^+ + \frac{i\gamma_2}{2}\hat{\sigma}_2^+ \hat{\sigma}_2^- \quad (24)
$$

is the effective NHH, and it may display HEPs. The last two terms in Eq. (23) are the quantum jumps.

In the classical or semiclassical regimes, the effect of the quantum jumps could be neglected directly. However, in the quantum regimes, quantum jumps have a profound effect on the dynamics of the system. According to quantum trajectory theory, if one postselects only those trajectories where no quantum jump takes place [67], the effective resulting dynamics of Eq. (23) is

$$
\dot{\rho} = -i(\hat{H}_{\text{eff}}\rho - \rho \hat{H}_{\text{eff}}^\dagger). \quad (25)
$$

It should be noted that this equation is not trace preserving and needs to be renormalized in calculation. Solving the Liouvillian equation Eq. (25), the density matrix operator can be expressed as [68]

$$
\rho(t) = e^{-i\hat{H}_{\text{eff}}t} \rho(0) e^{i\hat{H}_{\text{eff}}^\dagger t}. \quad (26)
$$

Supposing the eigenvalues of $\hat{H}_{\text{eff}}$ are h_k, and the corresponding eigenvectors are $|v_k\rangle$, one has

$$
\hat{H}_{\text{eff}}|v_k\rangle = h_k|v_k\rangle, \quad \langle v_k|\hat{H}_{\text{eff}}^\dagger = h_k^*\langle v_k|. \quad (27)
$$

According to Eq. (24), the eigenvalue spectrum of $\hat{H}_{\text{eff}}$ is

$$
h_1 = -\frac{i\gamma_1}{2}, \quad h_2 = -\frac{i\gamma_2}{2}, \quad h_{3,4} = -\frac{i}{2}\Gamma \pm \frac{1}{4}\delta, \quad (28)
$$

where

$$\Gamma = (\gamma_1 + \gamma_2)/2,$$

$$\delta = \sqrt{-(\gamma_1 + \gamma_2)^2 + 64\kappa^2}, \tag{29}$$

and the corresponding eigenvectors are

$$|v_1\rangle = (0 \quad 0 \quad 0 \quad 1)^T,$$

$$|v_2\rangle = (1 \quad 0 \quad 0 \quad 0)^T,$$

$$|v_3\rangle = \left(0 \quad \frac{i\gamma_1 + i\gamma_2 + \delta}{8} \quad 1 \quad 0\right)^T,$$

$$|v_4\rangle = \left(0 \quad \frac{i\gamma_1 + i\gamma_2 - \delta}{8} \quad 1 \quad 0\right)^T. \tag{30}$$

It can be seen from the eigenspectrum of $\hat{H}_{\text{eff}}$ that eigenvalues h_3 and h_4 and the corresponding eigenvectors are the same when $\delta = 0$, which manifests the existence of a second-order HEP. For fixed dissipative strength γ_1 and γ_2, when the value of coupling strength between the spins κ satisfies the condition

$$\kappa' = \frac{\gamma_1 + \gamma_2}{8} \tag{31}$$

the HEP appears.

In the following, we investigate the relation between the emergence of synchronization and HEPs. Without loss of generality, we choose $\langle \hat{\sigma}^x \rangle$ as the local observable to characterize the synchronization of the system. According to Eq. (26), the dynamics of $\langle \hat{\sigma}^x \rangle$ which has neglected the effect of quantum jumps can be expressed as

$$\left\langle \hat{\sigma}_j^x(t) \right\rangle = \text{Tr}[\hat{\sigma}_j^x \rho] = \text{Tr}\left[\hat{\sigma}_j^x e^{-i\hat{H}_{\text{eff}}t} \rho(0) e^{i\hat{H}_{\text{eff}}^\dagger t}\right]. \tag{32}$$

In Fig. 8, we show the dynamics of $\langle \hat{\sigma}_j^x(t) \rangle$ for two coupling strengths κ in the absence of quantum jumps. In Figs. 8(a) and 8(b), the interaction strength $\kappa = 0.001$ and 0.05, respectively, and the other system parameters are the same as those in Fig. 2. For $\gamma_1 = 0.02$ and $\gamma_2 = 0.01$, it can be obtained that HEP $\kappa' = 0.003\,75$ corresponding to $\delta = 0$. It can be seen from Fig. 8(a) that, for $\kappa = 0.001 < \kappa'$, $\langle \hat{\sigma}_1^x(t) \rangle$ and $\langle \hat{\sigma}_2^x(t) \rangle$ decrease as time evolves without oscillation. It can be seen from Fig. 8(b) that, for $\kappa = 0.05 > \kappa'$, $\langle \hat{\sigma}_1^x(t) \rangle$ and $\langle \hat{\sigma}_2^x(t) \rangle$ decrease with the same damped oscillation during the time evolution, and the curves of $\langle \hat{\sigma}_1^x(t) \rangle$ and $\langle \hat{\sigma}_2^x(t) \rangle$ are coincident. It is because the non-Hermitian Hamiltonian $\hat{H}_{\text{eff}}$ could exhibit only a single HEP, and the system displays a unique frequency when the coupling strength between the spins is greater than the HEP, which makes the system keep synchronized or antisynchronized during the whole evolution. It should be noted that, for a small value of κ, the oscillation of $\langle \hat{\sigma}_j^x(t) \rangle$ is not apparent and the decay is dominant. In this case, even $\langle \hat{\sigma}_1^x(t) \rangle$ and $\langle \hat{\sigma}_2^x(t) \rangle$ share a common oscillation frequency, and we cannot observe the phenomenon of synchronization. Comparing Fig. 8 with Fig. 2, it can be found that, in the presence of quantum jumps, the dynamical transition between synchronization and antisynchronization occurs, which is attributed to the existence of two different LEPs. It can be seen that the quantum jumps play an important role in the synchronization of the system. It is worth mentioning that different local observables make no qualitative difference on
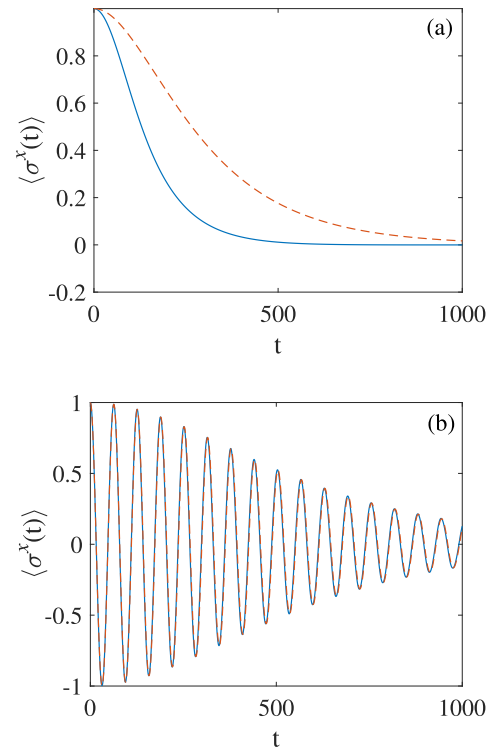

FIG. 8. The diagram of the local observable $\langle \hat{\sigma}_j^x \rangle$ as a function of t for different κ. The blue solid lines and orange dashed lines characterize $\langle \hat{\sigma}_1^x(t) \rangle$ and $\langle \hat{\sigma}_2^x(t) \rangle$, respectively. (a) $\kappa = 0.001$. (b) $\kappa = 0.05$. We set $\gamma_1 = 0.02$, $\gamma_2 = 0.01$.

the synchronization with HEP. Meanwhile, the initial state of the system would affect the amplitude and the phase of the local observables, but the phase difference between the spins is a constant, which makes the spins remain synchronized or antisynchronized in the whole evolution. The initial state of the system only determines whether the system is synchronized or antisynchronized.

IV. CONCLUSION

In this paper, we have investigated the synchronization of a spin chain locally coupled to dissipative environments with unbalanced gain and loss and explored the relation between the emergence of synchronization and exceptional points. By analyzing the Liouvillian spectrum governing the dynamics, we have found that the system exhibits LEPs. For our model in the Liouvillian formalism, the matrix of the Liouvillian superoperator is block diagonal and the different blocks correspond to the dynamics of different observables. We have found that $\hat{\sigma}^z$ corresponds to the block which has a single LEP, while $\hat{\sigma}^x$ and $\hat{\sigma}^y$ correspond to the block which has two LEPs. For $\hat{\sigma}^z$, when the coupling strength between the nearest spins is greater than the LEP it could get synchronized or antisynchronized. And for $\hat{\sigma}^x$ and $\hat{\sigma}^y$, when the coupling strength between the nearest spins is greater than both LEPs it could get synchronized or antisynchronized. And surprisingly as time evolves the spins can change from synchronization to antisynchronization and later change from antisynchronization back to synchronization again, i.e., a dynamical

transition between synchronization and antisynchronization occurs. Moreover, we have found that the initial state of the system does not affect the emergence of (anti)synchronization between the spins, but it would determine whether the system is synchronized or antisynchronized and affect the time at which the dynamical transition between synchronization and antisynchronization occurs.

We also consider the system dynamics of the effective non-Hermitian Hamiltonian by postselecting only those trajectories where no quantum jump takes place, and found that the effective non-Hermitian Hamiltonian has only a single HEP. When the coupling strength between the nearest spins is greater than the HEP, the system observables can get synchronized or antisynchronized and will keep (anti)synchronized during the whole evolution. Compared to the synchronization with LEPs which takes into account the effect of quantum jumps, it can be concluded that quantum jumps play an important role in the synchronization of the system.

APPENDIX A: LIOUVILLIAN SUPEROPERATOR

Due to the block structure of the Liouvillian superoperator, it can be decomposed into five different parts $\mathcal{L} = \oplus_\nu \mathcal{L}_\nu$, with $\nu \in \{a, b, c, d, e\}$ [66]. Each decomposed Liouvillian superoperator corresponds to a Hilbert-Schmidt subspace, $\mathcal{H} = \oplus_\nu \mathcal{H}_\nu$. $\mathcal{H}_a$ is spanned by $|eeee\rangle\rangle$, $|egeg\rangle\rangle$, $|egge\rangle\rangle$, $|geeg\rangle\rangle$, $|gege\rangle\rangle$, and $|gggg\rangle\rangle$; $\mathcal{H}_b$ is spanned by $|eeeg\rangle\rangle$, $|eege\rangle\rangle$, $|eggg\rangle\rangle$, and $|gegg\rangle\rangle$; $\mathcal{H}_c$ is spanned by $|egee\rangle\rangle$, $|geee\rangle\rangle$, $|ggeg\rangle\rangle$, and $|ggge\rangle\rangle$; $\mathcal{H}_d$ is spanned by $|eegg\rangle\rangle$; $\mathcal{H}_e$ is spanned by $|ggee\rangle\rangle$. In this way, the decomposed Liouvillian superoperators can be read as

$$
\mathcal{L}_a = \begin{pmatrix}
-\gamma_2 & 0 & 0 & 0 & \gamma_1 & 0 \\
\gamma_2 & 0 & 2i\kappa & -2i\kappa & 0 & \gamma_1 \\
0 & 2i\kappa & -\frac{1}{2}(\gamma_1 + \gamma_2) & 0 & -2i\kappa & 0 \\
0 & -2i\kappa & 0 & -\frac{1}{2}(\gamma_1 + \gamma_2) & 2i\kappa & 0 \\
0 & 0 & -2i\kappa & 2i\kappa & -\gamma_1 - \gamma_2 & 0 \\
0 & 0 & 0 & 0 & \gamma_2 & -\gamma_1
\end{pmatrix},
$$

$$
\mathcal{L}_b = \begin{pmatrix}
-\frac{1}{2}\gamma_2 & 2i\kappa & 0 & \gamma_1 \\
2i\kappa & -\frac{1}{2}\gamma_1 - \gamma_2 & 0 & 0 \\
0 & \gamma_2 & -\frac{1}{2}\gamma_1 & -2i\kappa \\
0 & 0 & -2i\kappa & -\gamma_1 - \frac{1}{2}\gamma_2
\end{pmatrix},
$$

$$
\mathcal{L}_c = \begin{pmatrix}
-\frac{1}{2}\gamma_2 & -2i\kappa & 0 & \gamma_1 \\
-2i\kappa & -\frac{1}{2}\gamma_1 - \gamma_2 & 0 & 0 \\
0 & \gamma_2 & -\frac{1}{2}\gamma_1 & 2i\kappa \\
0 & 0 & 2i\kappa & -\gamma_1 - \frac{1}{2}\gamma_2
\end{pmatrix}, \tag{A1}
$$

and $\mathcal{L}_d = \mathcal{L}_e = -\frac{1}{2}(\gamma_1 + \gamma_2)$.

APPENDIX B: LIOUVILLIAN SPECTRUM

In this section, we provide the full Liouvillian spectrum of $\mathcal{L}_\nu$, $\nu = \{a, b, c, d, e\}$. The explicit expressions of the eigenvalues λ_i^ν read

$$
\begin{aligned}
&\lambda_1^a = 0, \quad \lambda_{2,3}^a = -\frac{1}{2}(\gamma_1 + \gamma_2), \quad \lambda_4^a = -(\gamma_1 + \gamma_2), \quad \lambda_{5,6}^a = -\frac{1}{2}(\gamma_1 + \gamma_2 \pm \eta), \\
&\lambda_{1,2}^b = -\frac{1}{4}(2\gamma_1 + 2\gamma_2 \pm \sqrt{2}\sqrt{\alpha - \beta}), \quad \lambda_{3,4}^b = -\frac{1}{4}(2\gamma_1 + 2\gamma_2 \pm \sqrt{2}\sqrt{\alpha + \beta}), \\
&\lambda_{1,2}^c = -\frac{1}{4}(2\gamma_1 + 2\gamma_2 \pm \sqrt{2}\sqrt{\alpha - \beta}), \quad \lambda_{3,4}^c = -\frac{1}{4}(2\gamma_1 + 2\gamma_2 \pm \sqrt{2}\sqrt{\alpha + \beta}), \\
&\lambda_1^d = -\frac{1}{2}(\gamma_1 + \gamma_2), \quad \lambda_1^e = -\frac{1}{2}(\gamma_1 + \gamma_2).
\end{aligned} \tag{B1}
$$

And the corresponding right eigenmatrices ρ_i^y can be written as

$$
\rho_1^a = \begin{pmatrix} \frac{\gamma_1^2}{\gamma_2^2} & 0 & 0 & 0 \\ 0 & \frac{\gamma_1((\gamma_1+\gamma_2)^2+16\kappa^2)}{16\gamma_2^2\kappa^2} & \frac{i\gamma_1(\gamma_1+\gamma_2)}{4\gamma_2\kappa} & 0 \\ 0 & -\frac{i\gamma_1(\gamma_1+\gamma_2)}{4\gamma_2\kappa} & \frac{\gamma_1}{\gamma_2} & 0 \\ 0 & 0 & 0 & 1 \end{pmatrix}, \quad
\rho_2^a = \begin{pmatrix} -\frac{\gamma_1}{\gamma_2} & 0 & 0 & 0 \\ 0 & \frac{1}{2}(-1+\frac{\gamma_1}{\gamma_2}) & \frac{i(\gamma_1-\gamma_2)(\gamma_1+\gamma_2)}{8\gamma_2\kappa} & 0 \\ 0 & 0 & \frac{1}{2}(-1+\frac{\gamma_1}{\gamma_2}) & 0 \\ 0 & 0 & 0 & 1 \end{pmatrix},
$$

$$
\rho_3^a = \begin{pmatrix} 0 & 0 & 0 & 0 \\ 0 & 0 & 1 & 0 \\ 0 & 1 & 0 & 0 \\ 0 & 0 & 0 & 0 \end{pmatrix}, \quad
\rho_4^a = \begin{pmatrix} 1 & 0 & 0 & 0 \\ 0 & -1 & 0 & 0 \\ 0 & 0 & -1 & 0 \\ 0 & 0 & 0 & 1 \end{pmatrix},
$$

$$
\rho_{5,6}^a = \begin{pmatrix} \frac{\gamma_1(32\kappa^2-(\gamma_1-\gamma_2)(\gamma_1-\gamma_2\pm\eta))}{32\gamma_2\kappa^2} & 0 & 0 & 0 \\ 0 & \frac{(\gamma_1-\gamma_2\pm\eta)(\gamma_1^2+\gamma_1(-2\gamma_2\pm\eta)-\gamma_2(\gamma_2\pm\eta)-32\kappa^2)}{64\gamma_2\kappa^2} & \frac{i(\gamma_1(\gamma_1-\gamma_2\pm\eta)-32\kappa^2)}{8\gamma_2\kappa} & 0 \\ 0 & -\frac{i(\gamma_1(\gamma_1-\gamma_2\pm\eta)-32\kappa^2)}{8\gamma_2\kappa} & \frac{\gamma_1-\gamma_2\pm\eta}{2\gamma_2} & 0 \\ 0 & 0 & 0 & 1 \end{pmatrix},
$$

$$
\rho_{1,2}^b = \begin{pmatrix} 0 & 0 & 0 & 0 \\ \frac{32(\pm\sqrt{2}\sqrt{\alpha-\beta}+2\gamma_2)-\frac{(\pm\sqrt{2}\sqrt{\alpha-\beta}+2\gamma_1)(\beta-\gamma_1^2+\gamma_2^2+32\kappa^2)}{\kappa^2}}{128\gamma_2} & 0 & 0 & 0 \\ -\frac{i(-\beta+(\gamma_1-\gamma_2)(\pm\sqrt{2}\sqrt{\alpha-\beta}+\gamma_1-\gamma_2))}{16\gamma_2\kappa} & 0 & 0 & 0 \\ 0 & -\frac{i(\pm\sqrt{2}\sqrt{\alpha-\beta}+2\gamma_1)}{8\kappa} & 1 & 0 \end{pmatrix},
$$

$$
\rho_{3,4}^b = \begin{pmatrix} 0 & 0 & 0 & 0 \\ \frac{32(\pm\sqrt{2}\sqrt{\alpha+\beta}+2\gamma_2)+\frac{(\pm\sqrt{2}\sqrt{\alpha+\beta}+2\gamma_1)(\beta+\gamma_1^2-\gamma_2^2-32\kappa^2)}{\kappa^2}}{128\gamma_2} & 0 & 0 & 0 \\ -\frac{i(\beta+(\gamma_1-\gamma_2)(\pm\sqrt{2}\sqrt{\alpha+\beta}+\gamma_1-\gamma_2))}{16\gamma_2\kappa} & 0 & 0 & 0 \\ 0 & -\frac{i(\pm\sqrt{2}\sqrt{\alpha+\beta}+2\gamma_1)}{8\kappa} & 1 & 0 \end{pmatrix},
$$

$$
\rho_{1,2}^c = \begin{pmatrix} 0 & \frac{32(\pm\sqrt{2}\sqrt{\alpha-\beta}+2\gamma_2)-\frac{(\pm\sqrt{2}\sqrt{\alpha-\beta}+2\gamma_1)(\beta-\gamma_1^2+\gamma_2^2+32\kappa^2)}{\kappa^2}}{128\gamma_2} & \frac{i(-\beta+(\gamma_1-\gamma_2)(\pm\sqrt{2}\sqrt{\alpha-\beta}+\gamma_1-\gamma_2))}{16\gamma_2\kappa} & 0 \\ 0 & 0 & 0 & \frac{i(\pm\sqrt{2}\sqrt{\alpha-\beta}+2\gamma_1)}{8\kappa} \\ 0 & 0 & 0 & 1 \\ 0 & 0 & 0 & 0 \end{pmatrix},
$$

$$
\rho_{3,4}^c = \begin{pmatrix} 0 & \frac{32(\pm\sqrt{2}\sqrt{\alpha+\beta}+2\gamma_2)+\frac{(\pm\sqrt{2}\sqrt{\alpha+\beta}+2\gamma_1)(\beta+\gamma_1^2-\gamma_2^2-32\kappa^2)}{\kappa^2}}{128\gamma_2} & \frac{i(\beta+(\gamma_1-\gamma_2)(\pm\sqrt{2}\sqrt{\alpha+\beta}+\gamma_1-\gamma_2))}{16\gamma_2\kappa} & 0 \\ 0 & 0 & 0 & \frac{i(\pm\sqrt{2}\sqrt{\alpha+\beta}+2\gamma_1)}{8\kappa} \\ 0 & 0 & 0 & 1 \\ 0 & 0 & 0 & 0 \end{pmatrix},
$$

$$
\rho_1^d = \begin{pmatrix} 0 & 0 & 0 & 0 \\ 0 & 0 & 0 & 0 \\ 0 & 0 & 0 & 0 \\ 1 & 0 & 0 & 0 \end{pmatrix}, \quad
\rho_1^e = \begin{pmatrix} 0 & 0 & 0 & 1 \\ 0 & 0 & 0 & 0 \\ 0 & 0 & 0 & 0 \\ 0 & 0 & 0 & 0 \end{pmatrix}. \tag{B2}
$$

APPENDIX C: ANALYTICAL EXPRESSION OF $\langle \hat{\sigma}^x \rangle$

According to Eq. (10), when the coupling strength between the spins κ is greater than the second LEP κ_2^b, the local observable $\langle \hat{\sigma}_j^x \rangle$ can be derived as

$$
\begin{aligned}
\langle \hat{\sigma}_j^x \rangle &= \sum_{i=1}^{4} A_{ij} e^{\lambda_i^b t} \\
&= e^{-\Gamma t} (A_{1j} e^{i\omega_1 t} + A_{2j} e^{-i\omega_1 t} + A_{3j} e^{i\omega_2 t} + A_{4j} e^{-i\omega_2 t}) \\
&= e^{-\Gamma t} [A_{1j}(\cos \omega_1 t + i \sin \omega_1 t) + A_{2j}(\cos \omega_1 t - i \sin \omega_1 t) + A_{3j}(\cos \omega_2 t + i \sin \omega_2 t) + A_{4j}(\cos \omega_2 t - i \sin \omega_2 t)] \\
&= e^{-\Gamma t} [(A_{1j} + A_{2j}) \cos \omega_1 t + i(A_{1j} - A_{2j}) \sin \omega_1 t + (A_{3j} + A_{4j}) \cos \omega_2 t + i(A_{3j} - A_{4j}) \sin \omega_2 t] \\
&= e^{-\Gamma t} [A_j' \sin(\omega_1 t + \varphi_{1j}) + A_j'' \sin(\omega_2 t + \varphi_{2j})],
\end{aligned}
\tag{C1}
$$

where subscript $j = 1, 2$ denotes two different system spins, $A_{ij} = 2c_i^b \text{Tr}[\hat{\sigma}_j^x \rho_i^b]$, and $\Gamma = (\gamma_1 + \gamma_2)/2$:

$$
A_j' = \sqrt{(A_{1j} + A_{2j})^2 + [i(A_{1j} - A_{2j})]^2}, \quad A_j'' = \sqrt{(A_{3j} + A_{4j})^2 + [i(A_{3j} - A_{4j})]^2},
\tag{C2}
$$

$$
\varphi_{1j} = \arctan\left[\frac{A_{1j} + A_{2j}}{i(A_{1j} - A_{2j})} \right] + n\pi, \quad \varphi_{2j} = \arctan\left[\frac{A_{3j} + A_{4j}}{i(A_{3j} - A_{4j})} \right] + n\pi.
\tag{C3}
$$

It should be noted that $(A_{1j} + A_{2j})$, $i(A_{1j} - A_{2j})$, $(A_{3j} + A_{4j})$, and $i(A_{3j} - A_{4j})$ are all real. If $i(A_{1j} - A_{2j}) > 0$, $n = 0$, or else $n = 1$. Similarly, if $i(A_{3j} - A_{4j}) > 0$, $n = 0$, or else $n = 1$.

With the further increasing of the coupling strength between the spins, $\alpha \gg \beta$, it follows that $\alpha - \beta \approx \alpha + \beta$, which makes $\omega_1 + \omega_2 \gg \omega_1 - \omega_2$. It can be induced from Eq. (C1) that

$$
\begin{aligned}
\langle \hat{\sigma}_j^x \rangle &= e^{-\Gamma t} \Bigg[(A_j' + A_j'') \sin\left(\frac{\omega_1 + \omega_2}{2} t + \frac{\varphi_{1j} + \varphi_{2j}}{2} \right) \cos\left(\frac{\omega_1 - \omega_2}{2} t + \frac{\varphi_{1j} - \varphi_{2j}}{2} \right) \\
&\quad + (A_j' - A_j'') \cos\left(\frac{\omega_1 + \omega_2}{2} t + \frac{\varphi_{1j} + \varphi_{2j}}{2} \right) \sin\left(\frac{\omega_1 - \omega_2}{2} t + \frac{\varphi_{1j} - \varphi_{2j}}{2} \right) \Bigg] \\
&= \xi_j e^{-\Gamma t} \sin\left(\frac{\omega_1 + \omega_2}{2} t + \frac{\varphi_{1j} + \varphi_{2j}}{2} + \phi_j \right),
\end{aligned}
\tag{C4}
$$

where

$$
\xi_j = \sqrt{\left[(A_j' + A_j'') \cos\left(\frac{\omega_1 - \omega_2}{2} t + \frac{\varphi_{1j} - \varphi_{2j}}{2} \right) \right]^2 + \left[(A_j' - A_j'') \sin\left(\frac{\omega_1 - \omega_2}{2} t + \frac{\varphi_{1j} - \varphi_{2j}}{2} \right) \right]^2},
\tag{C5}
$$

$$
\phi_j = \arctan\left[\frac{(A_j' - A_j'') \sin\left(\frac{\omega_1 - \omega_2}{2} t + \frac{\varphi_{1j} - \varphi_{2j}}{2} \right)}{(A_j' + A_j'') \cos\left(\frac{\omega_1 - \omega_2}{2} t + \frac{\varphi_{1j} - \varphi_{2j}}{2} \right)} \right] + n\pi.
\tag{C6}
$$

If $(A_j' + A_j'') \cos(\frac{\omega_1 - \omega_2}{2} t + \frac{\varphi_{1j} - \varphi_{2j}}{2}) > 0$, $n = 0$, or else $n = 1$.

[1] A. Pikovsky, J. Kurths, M. Rosenblum, and J. Kurths, *Synchronization: A Universal Concept in Nonlinear Sciences* (Cambridge University, New York, 2003), Vol. 12.

[2] M. Kapitaniak, K. Czolczynski, P. Perlikowski, A. Stefanski, and T. Kapitaniak, Synchronization of clocks, Phys. Rep. **517**, 1 (2012).

[3] A. Arenas, A. Díaz-Guilera, J. Kurths, Y. Moreno, and C. Zhou, Synchronization in complex networks, Phys. Rep. **469**, 93 (2008).

[4] G. V. Osipov, J. Kurths, and C. Zhou, *Synchronization in Oscillatory Networks* (Springer, New York, 2007).

[5] L. Glass, Synchronization and rhythmic processes in physiology, Nature (London) **410**, 277 (2001).

[6] O. V. Zhirov and D. L. Shepelyansky, Quantum synchronization, European Physical Journal D **38**, 375 (2006).

[7] I. Goychuk, J. Casado-Pascual, M. Morillo, J. Lehmann, and P. Hänggi, Quantum stochastic synchronization, Phys. Rev. Lett. **97**, 210601 (2006).

[8] O. V. Zhirov and D. L. Shepelyansky, Synchronization and bistability of a qubit coupled to a driven dissipative oscillator, Phys. Rev. Lett. **100**, 014101 (2008).

[9] O. V. Zhirov and D. L. Shepelyansky, Quantum synchronization and entanglement of two qubits coupled to a driven dissipative resonator, Phys. Rev. B **80**, 014519 (2009).

[10] P. P. Orth, D. Roosen, W. Hofstetter, and K. Le Hur, Dynamics, synchronization, and quantum phase transitions

of two dissipative spins, Phys. Rev. B **82**, 144423 (2010).

[11] G. L. Giorgi, F. Galve, and R. Zambrini, Probing the spectral density of a dissipative qubit via quantum synchronization, Phys. Rev. A **94**, 052121 (2016).

[12] B. Bellomo, G. L. Giorgi, G. M. Palma, and R. Zambrini, Quantum synchronization as a local signature of super-and subradiance, Phys. Rev. A **95**, 043807 (2017).

[13] A. Cabot, G. Luca Giorgi, and R. Zambrini, Synchronization and coalescence in a dissipative two-qubit system, Proc. R. Soc. A **477**, 20200850 (2021).

[14] G. Karpat, I. Yalçınkaya, and B. Çakmak, Quantum synchronization in a collision model, Phys. Rev. A **100**, 012133 (2019).

[15] G. Karpat, I. Yalçınkaya, and B. Çakmak, Quantum synchronization of few-body systems under collective dissipation, Phys. Rev. A **101**, 042121 (2020).

[16] T. E. Lee, C.-K. Chan, and S. Wang, Entanglement tongue and quantum synchronization of disordered oscillators, Phys. Rev. E **89**, 022913 (2014).

[17] V. Ameri, M. Eghbali-Arani, A. Mari, A. Farace, F. Kheirandish, V. Giovannetti, and R. Fazio, Mutual information as an order parameter for quantum synchronization, Phys. Rev. A **91**, 012301 (2015).

[18] S. Walter, A. Nunnenkamp, and C. Bruder, Quantum synchronization of two van der Pol oscillators, Ann. Phys. (Leipzig) **527**, 131 (2015).

[19] N. Es'haqi-Sani, G. Manzano, R. Zambrini, and R. Fazio, Synchronization along quantum trajectories, Phys. Rev. Res. **2**, 023101 (2020).

[20] M. Xu, D. A. Tieri, E. C. Fine, J. K. Thompson, and M. J. Holland, Synchronization of two ensembles of atoms, Phys. Rev. Lett. **113**, 154101 (2014).

[21] A. Cabot, G. L. Giorgi, F. Galve, and R. Zambrini, Quantum synchronization in dimer atomic lattices, Phys. Rev. Lett. **123**, 023604 (2019).

[22] M. Ludwig and F. Marquardt, Quantum many-body dynamics in optomechanical arrays, Phys. Rev. Lett. **111**, 073603 (2013).

[23] M. R. Hush, W. Li, S. Genway, I. Lesanovsky, and A. D. Armour, Spin correlations as a probe of quantum synchronization in trapped-ion phonon lasers, Phys. Rev. A **91**, 061401(R) (2015).

[24] A. W. Laskar, P. Adhikary, S. Mondal, P. Katiyar, S. Vinjanampathy, and S. Ghosh, Observation of quantum phase synchronization in spin-1 atoms, Phys. Rev. Lett. **125**, 013601 (2020).

[25] M. Koppenhöfer, C. Bruder, and A. Roulet, Quantum synchronization on the IBM Q system, Phys. Rev. Res. **2**, 023026 (2020).

[26] L. Calderaro, A. Stanco, C. Agnesi, M. Avesani, D. Dequal, P. Villoresi, and G. Vallone, Fast and simple qubit-based synchronization for quantum key distribution, Phys. Rev. Appl. **13**, 054041 (2020).

[27] N. Jaseem, M. Hajdušek, V. Vedral, R. Fazio, L.-C. Kwek, and S. Vinjanampathy, Quantum synchronization in nanoscale heat engines, Phys. Rev. E **101**, 020201(R) (2020).

[28] G. L. Giorgi, A. Cabot, and R. Zambrini, Transient synchronization in open quantum systems, in *Advances in Open Systems and Fundamental Tests of Quantum Mechanics: Proceedings of the 684. WE-Heraeus-Seminar, Bad Honnef, Germany, 2–5 December 2018* (Springer, New York, 2019), pp. 73–89.

[29] M. Cattaneo, G. L. Giorgi, S. Maniscalco, G. S. Paraoanu, and R. Zambrini, Bath-induced collective phenomena on superconducting qubits: Synchronization, subradiance, and entanglement generation, Ann. Phys. (Leipzig) **533**, 2100038 (2021).

[30] H.-P. Breuer and F. Petruccione, *The Theory of Open Quantum Systems* (Oxford University, New York, 2002).

[31] G. Karpat, I. Yalçinkaya, B. Çakmak, G. L. Giorgi, and R. Zambrini, Synchronization and non-Markovianity in open quantum systems, Phys. Rev. A **103**, 062217 (2021).

[32] K.-J. Zhou, J. Zou, B.-M. Xu, L. Li, and B. Shao, Effect of non-Markovianity on synchronization, Commun. Theor. Phys. **73**, 105101 (2021).

[33] R. El-Ganainy, K. G. Makris, M. Khajavikhan, Z. H. Musslimani, S. Rotter, and D. N. Christodoulides, Non-Hermitian physics and PT symmetry, Nat. Phys. **14**, 11 (2018).

[34] C. M. Bender, Making sense of non-Hermitian Hamiltonians, Rep. Prog. Phys. **70**, 947 (2007).

[35] I. Rotter, A non-Hermitian Hamilton operator and the physics of open quantum systems, J. Phys. A **42**, 153001 (2009).

[36] W. Heiss, The physics of exceptional points, J. Phys. A **45**, 444016 (2012).

[37] T. Kato, *Perturbation Theory for Linear Operators* (Springer, New York, 2013), Vol. 132.

[38] H. Hodaei, A. U. Hassan, S. Wittek, H. Garcia-Gracia, R. El-Ganainy, D. N. Christodoulides, and M. Khajavikhan, Enhanced sensitivity at higher-order exceptional points, Nature (London) **548**, 187 (2017).

[39] W. Chen, Ş. Kaya Özdemir, G. Zhao, J. Wiersig, and L. Yang, Exceptional points enhance sensing in an optical microcavity, Nature (London) **548**, 192 (2017).

[40] J. Wiersig, Review of exceptional point-based sensors, Photonics Research **8**, 1457 (2020).

[41] Y.-H. Lai, Y.-K. Lu, M.-G. Suh, Z. Yuan, and K. Vahala, Observation of the exceptional-point-enhanced Sagnac effect, Nature (London) **576**, 65 (2019).

[42] M. P. Hokmabadi, A. Schumer, D. N. Christodoulides, and M. Khajavikhan, Non-Hermitian ring laser gyroscopes with enhanced Sagnac sensitivity, Nature (London) **576**, 70 (2019).

[43] B. Peng, Ş. K. Özdemir, M. Liertzer, W. Chen, J. Kramer, H. Yılmaz, J. Wiersig, S. Rotter, and L. Yang, Chiral modes and directional lasing at exceptional points, Proc. Natl. Acad. Sci. USA **113**, 6845 (2016).

[44] S. Soleymani, Q. Zhong, M. Mokim, S. Rotter, R. El-Ganainy, and Ş. Özdemir, Chiral and degenerate perfect absorption on exceptional surfaces, Nat. Commun. **13**, 599 (2022).

[45] B. Peng, Ş. Özdemir, S. Rotter, H. Yilmaz, M. Liertzer, F. Monifi, C. Bender, F. Nori, and L. Yang, Loss-induced suppression and revival of lasing, Science **346**, 328 (2014).

[46] F. Minganti, A. Biella, N. Bartolo, and C. Ciuti, Spectral theory of Liouvillians for dissipative phase transitions, Phys. Rev. A **98**, 042118 (2018).

[47] F. Minganti, A. Miranowicz, R. W. Chhajlany, I. I. Arkhipov, and F. Nori, Hybrid-Liouvillian formalism connecting exceptional points of non-Hermitian Hamiltonians and Liouvillians via postselection of quantum trajectories, Phys. Rev. A **101**, 062112 (2020).

[48] S. Haroche and J.-M. Raimond, *Exploring the Quantum: Atoms, Cavities, and Photons* (Oxford University, New York, 2006).

[49] H. M. Wiseman and G. J. Milburn, *Quantum Measurement and Control* (Cambridge University, New York, 2009).

[50] F. Minganti, A. Miranowicz, R. W. Chhajlany, and F. Nori, Quantum exceptional points of non-Hermitian Hamiltonians and Liouvillians: The effects of quantum jumps, Phys. Rev. A **100**, 062131 (2019).

[51] H. M. Wiseman, Quantum trajectories and quantum measurement theory, Quantum Semiclass. Opt. **8**, 205 (1996).

[52] A. J. Daley, Quantum trajectories and open many-body quantum systems, Adv. Phys. **63**, 77 (2014).

[53] H. Jing, S. K. Özdemir, X.-Y. Lü, J. Zhang, L. Yang, and F. Nori, PT-symmetric phonon laser, Phys. Rev. Lett. **113**, 053604 (2014).

[54] F. Minganti, D. Huybrechts, C. Elouard, F. Nori, and I. I. Arkhipov, Creating and controlling exceptional points of non-Hermitian Hamiltonians via homodyne Lindbladian invariance, Phys. Rev. A **106**, 042210 (2022).

[55] N. Hatano, Exceptional points of the Lindblad operator of a two-level system, Mol. Phys. **117**, 2121 (2019).

[56] I. I. Arkhipov, A. Miranowicz, F. Minganti, and F. Nori, Liouvillian exceptional points of any order in dissipative linear bosonic systems: Coherence functions and switching between PT and anti-PT symmetries, Phys. Rev. A **102**, 033715 (2020).

[57] S. Khandelwal, N. Brunner, and G. Haack, Signatures of Liouvillian exceptional points in a quantum thermal machine, PRX Quantum **2**, 040346 (2021).

[58] G. Benenti, G. Casati, T. Prosen, and D. Rossini, Negative differential conductivity in far-from-equilibrium quantum spin chains, Europhys. Lett. **85**, 37001 (2009).

[59] T. Prosen, Open XXZ spin chain: Nonequilibrium steady state and a strict bound on ballistic transport, Phys. Rev. Lett. **106**, 217206 (2011).

[60] T. Prosen, PT-symmetric quantum Liouvillean dynamics, Phys. Rev. Lett. **109**, 090404 (2012).

[61] F.-H. Ren, Z.-M. Wang, and Y.-J. Gu, Quantum state transfer through a spin chain in two non-Markovian baths, Quant. Info. Proc. **18**, 193 (2019).

[62] J. J. Mendoza-Arenas, S. R. Clark, and D. Jaksch, Coexistence of energy diffusion and local thermalization in nonequilibrium XXZ spin chains with integrability breaking, Phys. Rev. E **91**, 042129 (2015).

[63] F. Benatti, R. Floreanini, and L. Memarzadeh, Bath-assisted transport in a three-site spin chain: Global versus local approach, Phys. Rev. A **102**, 042219 (2020).

[64] F. Benatti, R. Floreanini, and L. Memarzadeh, Stationary states of open XX-spin chains, Phys. Rev. A **106**, 062218 (2022).

[65] F. Benatti, R. Floreanini, and L. Memarzadeh, Exact steady state of the open XX-spin chain: Entanglement and transport properties, PRX Quantum **2**, 030344 (2021).

[66] M. Cattaneo, G. L. Giorgi, S. Maniscalco, and R. Zambrini, Symmetry and block structure of the Liouvillian superoperator in partial secular approximation, Phys. Rev. A **101**, 042108 (2020).

[67] M. Naghiloo, M. Abbasi, Y. N. Joglekar, and K. Murch, Quantum state tomography across the exceptional point in a single dissipative qubit, Nat. Phys. **15**, 1232 (2019).

[68] G.-Q. Zhang, Z. Chen, D. Xu, N. Shammah, M. Liao, T.-F. Li, L. Tong, S.-Y. Zhu, F. Nori, and J. Q. You, Exceptional point and cross-relaxation effect in a hybrid quantum system, PRX Quantum **2**, 020307 (2021).